JOURNAL OF SOLID STATE CHEMISTRY 115, 469–475 (1995)

Ordered Substitution of Iron for Copper in the Tetragonal Perovskite $La_{6.4}Sr_{1.6}Cu_8O_{20}$

R. Genouel, C. Michel, N. Nguyen, M. Hervieu, and B. Raveau

Laboratoire CRISMAT, CNRS URA 1318-ISMRA, Université de Caen, Boulevard du Maréchal Juin, 14050 Caen Cedex, France

Received May 5, 1994; in revised form August 30, 1994; accepted September 6, 1994

Two series of iron-substituted cuprates with the tetragonal $La_{6.4}Sr_{1.6}Cu_8O_{20}$ oxygen deficient perovskite structure have been isolated: $La_{6.4}Sr_{1.6}Cu_{8-x}Fe_xO_{20}$ ($0 \le x \le 1.20$) and $La_{6.4-x}Sr_{1.6+x}Cu_{8-x}Fe_xO_{20}$ ($0 \le x \le 2$). The XRD and Mössbauer studies show that they correspond to a preferential substitution of Fe(III) for copper in the octahedral sites of the structure. In fact the ideal structure can be described as 90°-oriented "123" copper ribbons interconnected with $[FeO_3]_\infty$ rows of FeO_6 octahedra. The transport properties of these phases show a transition from a metallic to a semiconducting state. The difference in behavior between the $La_{6.4}Sr_{1.6}Cu_{8-x}Fe_xO_{20}$ series and the $La_{6.4-x}Sr_{1.6+x}Cu_{8-x}Fe_xO_{20}$ series is interpreted on the basis of hole carrier density introduced by Cu(III) and of the trapping of carriers by Fe(III) species. The possibility of anisotropic transport properties with a metallic conductivity along c is discussed. © 1995 Academic Press, Inc.

INTRODUCTION

Numerous studies of the substitution of iron for copper in layered cuprates related to the perovskite have been performed these past years in order to understand the relationships between magnetism and superconductivity in these compounds. This is indeed the case for the Fe-substituted "123" structures (1–5). In this respect the cuprate $La_{8-x}Sr_xCu_8O_{20}$ (6, 7), although it does not superconduct, is an interesting candidate for the study of the influence of iron substitution on magnetism and conductivity. Like $YBa_2Cu_3O_7$, this phase is an ordered oxygen-deficient perovskite, but the distribution of the anionic vacancies causes the $[Cu_8O_{20}]_\infty$ framework (Fig. 1) to consist of rows of CuO_6 octahedra and CuO_5 pyramids running along **c**, interconnected by rows of CuO_4 square planar groups. As a result this framework is tridimensional and exhibits a metallic behavior (7) due to the Cu(II)–Cu(III) mixed valence but does not superconduct.

The ability of trivalent iron to adopt the octahedral coordination and to a lesser degree the pyramidal coordination suggests that it should be possible to replace copper with iron in an ordered way in order to break the tridimensional conductivity, and to create an unidimensional conducting behavior along **c**. We describe herein the structural, magnetic, and transport properties of two series of iron-substituted oxides, $La_{6.4}Sr_{1.6}Cu_{8-x}Fe_xO_{20}$ and $La_{6.4-x}Sr_{1.6+x}Cu_{8-x}Fe_xO_{20}$, that belong to this family.

EXPERIMENTAL

Two series of oxides were studied corresponding to the ideal formula: $La_{6.4}Sr_{1.6}Cu_{8-x}Fe_xO_{20}$ and $La_{6.4-x}Sr_{1.6+x}Cu_{8-x}Fe_xO_{20}$. The syntheses were realized by solid state reaction from predried oxides La_2O_3, CuO, Fe_2O_3, and strontium carbonate, mixed in stoichiometric ratios. The mixtures were heated in a platinum crucible in air at 1000°C for 24 hr and then quenched to room temperature. After regrinding, the thermal treatment was repeated once.

The lattice constants and structure were determined by Rietveld method (computer program DBW 3.2 (8)) from X-ray powder diffraction patterns obtained with a Philips goniometer using Cu$K\alpha$ radiation. Data were collected by step scanning in the range $10° \le 2\theta \le 100°$ with an increment of 0.02° (2θ).

The oxygen content was determined by chemical analysis using a redox back titration method. Tetravalent iron and trivalent copper species, if they exist, were reduced into Fe(III) and Cu(II) by a known amount of iron (II) chloride in an acid solution. The amount of unreacted Fe(II) was then determined by titration with potassium dichromate.

The magnetic susceptibility was measured by the Faraday method in the temperature range $77\ K \le T \le 700\ K$ using a Setaram MTB 10-8 balance. The Mössbauer resonance spectra were recorded at room temperature using a constant acceleration spectrometer with a $^{57}Co/Rh$ source in a transmission geometry. The isomer shifts are given with respect to metallic iron at room temperature. Resistivity measurements were performed in the temperature range 20–290 K using a classical four-probe method on samples sintered in the form of bars ($12 \times 2 \times 1\ mm^3$) under the same conditions as the syntheses (as-prepared samples). Postannealing treatments were performed at

0022-4596/95 $6.00

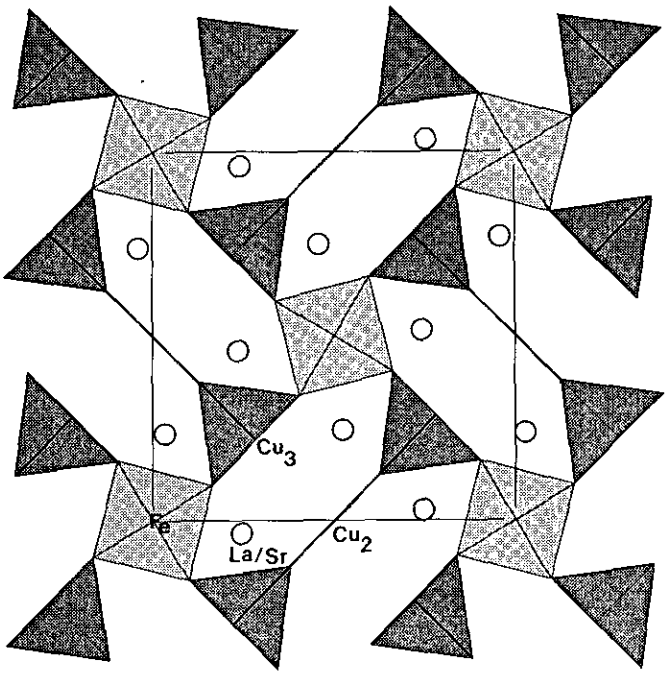

FIG. 1. Projection onto the (001) plane of the framework of the tetragonal oxygen-deficient perovskite $La_{6.4}Sr_{1.6}Cu_8O_{20}$.

450°C on the as-prepared samples in oxygen flow (O_2 samples), under 10 bar oxygen pressure ($10bO_2$ samples) bar oxygen pressure ($100bO_2$ samples).

RESULTS AND DISCUSSION

Structural Properties

For the above-described experimental conditions, single-phased materials can be obtained for $0 \leq x \leq 1.2$ and $0 \leq x \leq 2$ for the series $La_{6.4}Sr_{1.6}Cu_{8-x}Fe_xO_{20-\varepsilon}$ and $La_{6.4-x}Sr_{1.6+x}Cu_{8-x}Fe_xO_{20-\varepsilon}$, respectively. The chemical analyses show that for each series, the oxygen content remains approximately constant for the as-synthesized samples and close to 20 oxygen atoms per cell in the limit of the experimental error, i.e., $\varepsilon \approx 0 \pm 0.05$. Postannealing treatments do not allow one to detect any significant variation of the oxygen content, showing that the oxygen nonstoichiometry ε, if it exists, is probably very small. Note that postannealing treatments under 100 bar oxygen pressure lead to the destruction of the structure for the simple substituted materials. The powder X-ray diffraction patterns of the as-prepared samples are isotypic with that of the limit $x = 0$ (6). Thus, they can be indexed in a tetragonal cell with parameters closely related to the cubic perovskite cell: $a \sim 2a_p\sqrt{2}$, $c \sim a_p$. This is confirmed by electron diffraction which elucidates the reflection conditions, $0kl: k = 2n$, allowing the three possible space groups $P\bar{4}b2$, $P4bm$, and $P4/mbm$. The evolution of the lattice constants is plotted in Fig. 2 for the two series. In both cases, the a parameter decreases as x increases (Fig. 2a) whereas the c parameter increases (Fig. 2b). However, the variation amplitude is smaller for a and is larger for c in the case of the single substitution ($La_{6.4}Sr_{1.6}Cu_{8-x}Fe_xO_y$ series) than in the case of the double substitution ($La_{6.4-x}Sr_{1.6+x}Cu_{8-x}Fe_xO_y$ series). It results in the cell volume increasing with x for the single substituted materials whereas it tends to decrease for the double substituted materials (Fig. 2c). Note also that the lattice constants do not vary significantly after postannealing in oxygen (Table 1). This confirms that the oxygen nonstoichiometry is small and does not affect the cell parameters.

Thus, the structural evolution is easily explained by the relative size of the species participating in the

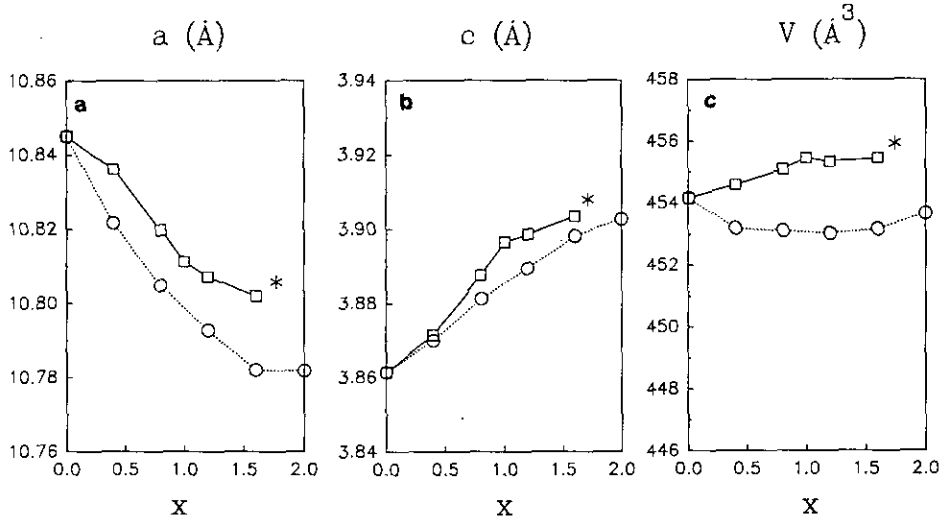

FIG. 2. Evolution of a parameter (a), c parameter (b), and volume (c) versus x in the oxides $La_{6.4}Sr_{1.6}Cu_{8-x}Fe_xO_{20}$ (dotted lines). The asterisk indicates a multiphased system.

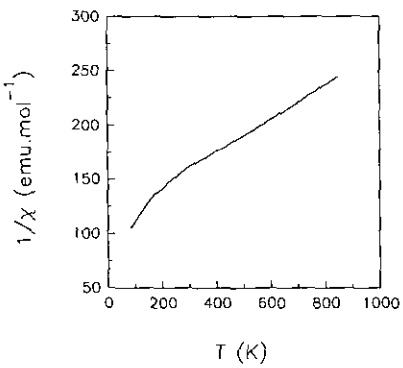

FIG. 3. χ_M^{-1} (emu/mole) versus T (K) for the composition $La_{4.4}Sr_{3.6}Cu_6Fe_2O_{20}$.

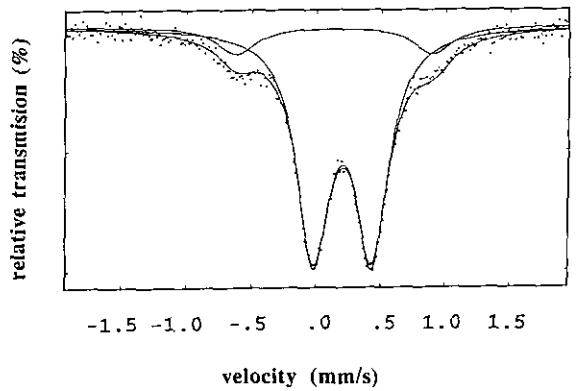

FIG. 4. Mössbauer spectrum recorded at room temperature for $La_{4.4}Sr_{3.6}Cu_6Fe_2O_{20}$.

$[Cu_{8-x}Fe_xO_{20}]_\infty$ framework. In the $La_{6.4}Sr_{1.6}Cu_{8-x}Fe_xO_{20}$ series, the increase in the cell volume is in agreement with the replacement of Cu(III) by the bigger species Fe(III). In $La_{6.4-x}Sr_{1.6+x}Cu_{8-x}Fe_xO_{20}$, two opposite effects can explain the slight decrease in the cell volume: the replacement of La^{3+} by Sr^{2+} that tends to increase the parameters, and the replacement of Cu(II) by the smaller species Fe(III) that tends to decrease the parameters.

Based on the oxygen content O_{20} deduced from the chemical analysis, the maximum limit of substitution in $La_{6.4}Sr_{1.6}Cu_{8-x}Fe_xO_{20}$ should be $x = 1.6$. For this value, impurity peaks were detected, so that only the limit value $x = 1.2$ could be reached. For the second series, $La_{6.4-x}Sr_{1.6+x}Cu_{8-x}Fe_xO_{20}$, the charge balance does not limit the amount of Fe(III) that may enter into the structure. The limit of substitution $x = 2$ suggests that in this structure Fe(III) is preferentially located in the octahedral sites in agreement with the fact that the octahedral sites (2*a*) may be completely occupied by iron. Nevertheless the possibility of Fe(III) occupying the two other (2*d*) pyramidal sites of the structure cannot be ruled out. In order to shed light on this issue, the limit compound $La_{4.4}Sr_{3.6}Cu_6Fe_2O_{20}$ was investigated using susceptibility measurements and Mössbauer spectroscopy.

The susceptibility measurements performed in the range 77–700 K show a linear dependence of χ_M^{-1} versus T above 300 K (Fig. 3). The magnetic moment per iron mole $\bar{\mu}_{exp}$(Fe) deduced from the linear part of the curve ($\bar{\mu}_{exp}$(Fe) = 6.0 μ_B) is in perfect agreement with the expected value of 5.9 μ_B for Fe(III). The Mössbauer data were recorded at room temperature. The spectrum consists of two paramagnetic doublets (Fig. 4) corresponding to two different environments. Their isomer shifts are characteristic of Fe(III) species (Table 2). The first site (86%) with SQ = 0.45 mm/sec corresponds to an octahedral environment. However, the large value of SQ = 1.52 mm/sec of the second site (14%) shows that this second Fe(III) species exhibits a square pyramidal environment. A spectrum recorded with a large velocity range −10 mm/sec $\leq v \leq$ +10 mm/sec does not show any additional peaks indicating that the outer lines in the paramagnetic spectrum do not belong to a magnetic site.

This result strongly supports the model of the ordered distribution of iron, located on the octahedral sites of the structure. Thus the ideal structure of the limit phase $La_{4.4}Sr_{3.6}Cu_6Fe_2O_{20}$, can be described as being built up from 90° oriented "123" type ribbons (Fig. 1) running along **c**, interconnected through $[FeO_3]_\infty$ rows of FeO_6 octahedra. In this way such a structure can be considered unidimensional from the viewpoint of the copper polyhedra, the conductivity being broken in the (001) plane by the Fe(III) octahedra. The presence of small amounts of iron on pyramidal copper (14%) can be due either to a partial disordering of iron, that would go into the pyrami-

TABLE 1
Lattice Constants and Cell Volume after Annealing Treatments in Oxygen Compared to As-Synthesized Sample Parameters

	As-synthesized			O_2			10b O_2		
Composition	a (Å)	c (Å)	V (Å^3)	a (Å)	c (Å)	V (Å^3)	a (Å)	c (Å)	V (Å^3)
$La_{6.4}Sr_{1.6}Cu_{6.8}Fe_{1.2}O_{20}$	10.8072(6)	3.8987(3)	455.2	10.8065(5)	3.8992(2)	455.3	10.8080(3)	3.8988(1)	455.4
$La_{4.8}Sr_{3.2}Cu_{6.4}Fe_{1.6}O_{20}$	10.7820(6)	3.8980(2)	453.1	10.7800(4)	3.8965(2)	452.8	10.7805(2)	3.8974(1)	452.9
$La_{4.4}Sr_{3.6}Cu_6Fe_2O_{20}$	10.7807(4)	3.9026(1)	453.6	10.7795(4)	3.9012(2)	453.3	10.7770(3)	3.9031(1)	453.3

dal Cu(3) sites, or to a small oxygen deficiency, on the oxygen O(1) sites that form the CuO_6 octahedra. A small oxygen deficiency with respect to the ideal formula $La_{4.4}Sr_{3.6}Cu^{II}_{4.4}Cu^{III}_{1.6}Fe^{III}_2O_{20}$ can indeed explain the second hypothesis.

The study of the structure of this limit phase from powder X-ray data confirms the ordered distribution of iron and copper deduced from Mössbauer spectroscopy. The calculations were performed in the same space group as for the study of the cuprate $La_{6.4}Sr_{1.6}Cu_8O_{20}$ (6): *P4/mbm* (152 possible *hkl* in the range $10° \leq 2\theta \leq 100°$). Position parameters for all the atoms and isotropic thermal factors for metallic elements were successively refined, the thermal factors of the oxygen atoms being arbitrarily fixed to 1 Å^2. Two limit models were considered: in the first one, copper and iron were randomly distributed over the octahedral and pyramidal sites (2*a* and 4*g* sites, respectively); in the second one, iron was located only in the octahedral sites. After refinement of the different variables, both models led to indentical conventional *R* profile factors using raw intensities ($R_p = 0.0598$, $R_{wp} = 0.0761$, $\chi^2 = 2.12$) and to very close *R* intensity factor ($R_i = 0.053$ and $R_i = 0.050$ for the first and the second model respectively). However, the examination of the *B* factors showed that in the first model, the value for the elements in octahedral environment was high ($B = 0.94$ Å^2) compared to those in a pyramidal or square planar environment which were slightly negative ($B = -0.1$ Å^2), whereas in the second model, all *B* values were found to be positive and very close ($B = 0.1$–0.2 Å^2). Although they cannot be considered as proof of the ordering, these results confirm the proposed model, especially if one keeps in mind the close scattering factors of iron and copper. The atomic coordinates (Table 3) and interatomic distances (Table 4) are close to those of the pure copper phase $La_{6.4}Sr_{1.6}Cu_8O_{20}$ (6). Note that the interatomic distances in the CuO_5 pyramids are characteristic of copper with a larger Cu–O apical distance, which shows that this site cannot be mainly occupied by iron, taking into consideration our previous results on $YBaFeCuO_5$ (9, 10). The experimental calculated and difference X-ray diffraction patterns (Fig. 5) attest the quality of the refinements.

TABLE 2
Mössbauer Parameters at Room Temperature for $La_{4.4}Sr_{3.6}Cu_6Fe_2O_{20}$

Composition	IS (mm · sec^{-1})	Γ (mm · sec)$^{-1}$	SQ (mm · sec^{-1})	%
$x = 2$	0.31(1)	0.31(1)	0.45(1)	86
	0.25(1)	0.37(1)	1.52(2)	14

Note. IS, isomer shift related to iron metal; Γ, full width at half-maximum; SQ, quadrupolar splitting; and %, fitted intensity.

TABLE 3
Refined Parameters for $La_{4.4}Sr_{3.6}Cu_6Fe_2O_{20}$ (Space Group: *P4/mbm*)

Atom	Sites	*x*	*y*	*z*	*B* (Å^2)
La(Sr)	8*j*	0.2567(2)	0.4723(1)	0.5	0.72(4)
Fe	2*a*	0.0	0.0	0.0	0.1(2)
Cu2	2*d*	0.5	0.0	0.0	0.1(2)
Cu3	4*g*	0.2244(3)	0.5 + *x*	0.0	0.2(1)
O1	2*b*	0.0	0.0	0.5	1.00
O2	2*c*	0.5	0.0	0.5	1.00
O3	4*h*	0.211(1)	0.5 + *x*	0.5	1.00
O4	4*g*	0.283(2)	0.5 + *x*	0.0	1.00
O5	8*i*	0.153(1)	0.094(2)	0.0	1.00

Note. $R_p = 0.0598$, $R_{wp} = 0.0761$, and $R_i = 0.050$.

Transport Properties

The conductivity versus temperature was measured for both series, in the temperature range 20–290 K. Room temperature measurements of the conductivity for different compositions are listed in Table 5 for different thermal treatments, i.e., as-synthesized samples and samples annealed in oxygen at different pressures. The first important feature elucidated from this table is that the conductivity of the $La_{6.4}Sr_{1.6}Cu_{8-x}Fe_xO_{20}$ sample is not significantly affected by the oxygen postannealing treatments; this shows that the hole carrier density is not affected and confirms that the as-synthesized sample is O_{20} stoichiometric. In the case of the $La_{6.4-x}Sr_{1.6+x}Cu_{8-x}Fe_xO_{20-\varepsilon}$ samples, a significant increase of the conductivity is observed by oxygen annealing; nevertheless, the variation is much less than one order of magnitude. This supports strongly our hypothesis deduced from the Mössbauer study suggesting that part of the CuO_6 octahedra

TABLE 4
Interatomic Distances

	d(Å)	
La(Sr)–O(1)	2.640(2)	×1
–O(2)	2.784(2)	×1
–O(3)	2.623(9)	×1
–O′(3)	2.835(9)	×1
–O(4)	2.647(8)	×2
–O(5)	2.546(8)	×2
–O′(5)	2.867(9)	×2
Fe–O(1)	1.951(1)	×2
–O(5)	1.935(9)	×4
Cu2–O(2)	1.951(1)	×2
–O(4)	1.781(9)	×2
Cu3–O(3)	1.962(1)	×2
–O(4)	2.421(9)	×1
–O(5)	1.931(9)	×2

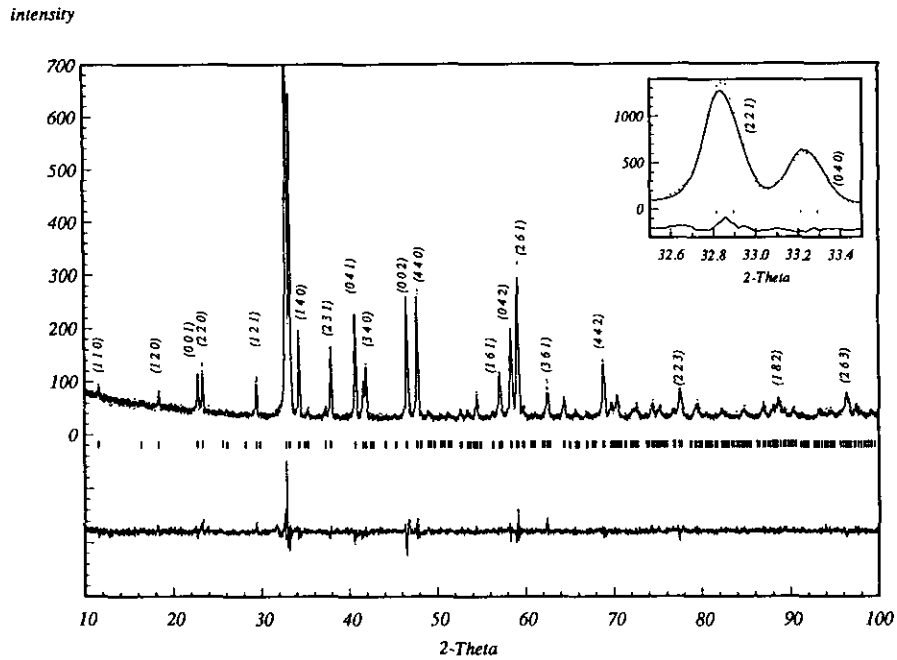

FIG. 5. Experimental (dotted line) and calculated (solid line) X-ray diffraction patterns of $La_{4.4}Sr_{3.6}Cu_6Fe_2O_{20}$, with indices for some diffraction peaks. Small bars indicate the Bragg angle positions. At the bottom of the figure, the difference X-ray pattern is plotted. The inset shows the intensities and Bragg angles positions of the (221) and (040) peaks.

is oxygen deficient. Thus this second series is oxygen substoichiometric $O_{20-\varepsilon}$ when as-synthesized; as a result, oxygen annealing allows ε to be decreased, i.e., the hole carrier density, and consequently allows the conductivity to be increased.

The second important point deals with the decrease of the conductivity with increasing the iron content. For both series one indeed observes (Fig. 6) a transition from a metallic to a semimetallic behavior as x increases. This behavior has already been observed for the iron-substituted "123" cuprate (1). But most interesting is the fact that the effect of substitution upon conductivity is much less pronounced for the double substituted phase $La_{6.4-x}Sr_{1.6+x}Cu_{8-x}Fe_xO_{20-\varepsilon}$ (Fig. 6b) than for the single substituted phase $La_{6.4}Sr_{1.6}Cu_{8-x}Fe_xO_{20}$ (Fig. 6a). The transition to a semiconductor appears at $x = 1$ for the oxide $La_{6.4}Sr_{1.6}Cu_{8-x}Fe_xO_{20}$ (Fig. 6a), whereas at $x = 1.2$, $La_{6.4-x}Sr_{1.6+x}Cu_{8-x}Fe_xO_{20}$ (Fig. 6b) still exhibits a metallic behavior. In the same way, for a given x value, $x = 1$, the conductivity of the oxygen-annealed doubly substituted

TABLE 5

Room Temperature Electrical Resistivity (in Ω · cm) for Some Compositions of the Series $La_{6.4}Sr_{1.6}Cu_{8-x}Fe_xO_{20}$ and $La_{6.4-x}Sr_{1.6+x}Cu_{8-x}Fe_xO_{20}$ after Synthesis and Postannealing Treatments

	As-prepared	O_2	$10bO_2$	$100bO_2$
$La_{6.4}Sr_{1.6}Cu_8O_{20}$	1.7×10^{-3}	1.6×10^{-3}	1.3×10^{-3}	1.1×10^{-3}
$La_{6.4}Sr_{1.6}Cu_{8-x}Fe_xO_{20}$				
$x = 1$	3.1×10^{-2}	3.4×10^{-2}	2.8×10^{-2}	[a]
$x = 1.2$	1.2×10^{-1}	9.8×10^{-2}	1.3×10^{-1}	[a]
$La_{6.4-x}Sr_{1.6+x}Cu_{8-x}Fe_xO_{20}$				
$x = 1$	4×10^{-3}	2.4×10^{-3}	2.3×10^{-3}	2.5×10^{-3}
$x = 1.2$	7×10^{-3}	4.1×10^{-3}	3.2×10^{-3}	3.1×10^{-3}
$x = 1.6$	1.7×10^{-2}	4.5×10^{-3}	3.8×10^{-3}	4.3×10^{-3}
$x = 2.0$	1.9×10^{-2}	6.3×10^{-3}	6.2×10^{-3}	6.1×10^{-3}

[a] Decomposed material.

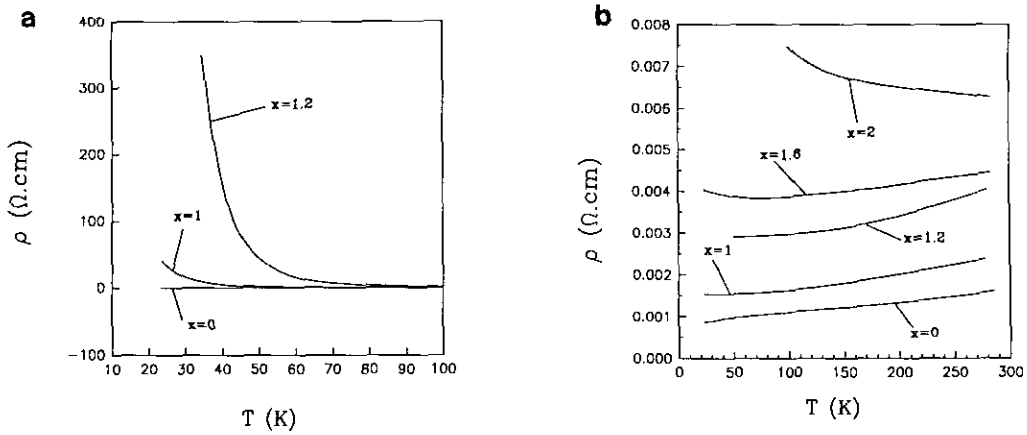

FIG. 6. Resistivity $\rho(\Omega \cdot \text{cm})$ versus T (K) for some as-synthesized compositions of the series $La_{6.4}Sr_{1.6}Cu_{8-x}Fe_xO_{20}$ (a) and of the series $La_{6.4-x}Sr_{1.6+x}Cu_{8-x}Fe_xO_{20}$ (b).

phase is 14 times higher than that of the simply substituted cuprate, whereas a factor of 24 is observed for $x = 1.2$ (Table 5). Two factors must be taken into consideration to explain this evolution of the conductivity. The first one deals with the hole carrier density which imposes that a critical Cu(III) content is necessary for the appearance of a metallic behavior. The second factor deals with the fact that simply introducing an alien element, like Fe(III), in the copper sites tends to trap the carriers and consequently progressively breaks the conductivity. The first factor has a predominant role in the dramatic decrease in conductivity in the first series, since Fe(III) replaces continuously Cu(III), according to the formula $La_{6.4}Sr_{1.6}Cu^{II}_{6.4}Cu^{III}_{1.6-x}Fe^{III}_xO_{20}$. Consequently, a semiconducting or insulating behavior would be expected for the limit phase, $x = 1.6$, that would contain only Cu(II), as shown for instance for the layered oxygen deficient perovskites $LnBaFe^{III}Cu^{II}O_5$ (Ln = Gd, Y) (9, 10), that exhibits a very low conductivity of about 10^{-5} $(\Omega \cdot \text{cm})^{-1}$ at room temperature. Although this limit $x = 1.6$ could not be reached, it appears clearly that for $x = 1.2$ (Fig. 6a), the conductivity has dramatically decreased by two order of magnitudes with respect to the phase $La_{6.4}Sr_{1.6}Cu_8O_{20}$ at room temperature (Table 5). In the second series, the coupled substitution "La–Sr, Cu–Fe" introduces a compensation effect so that the hole carrier density should not vary according to the ideal formulation $La_{6.4-x}Sr_{1.6+x}Cu^{II}_{6.4-x}Cu^{III}_{1.6}Fe^{III}_xO_{20}$. A small oxygen deficiency is in fact detected from the conductivity measurements, leading to the $O_{20-\varepsilon}$ formula, but clearly the decrease of conductivity is not due to the decrease of the hole carrier density, especially for the oxygen annealed samples. Thus the main factor that governs the decrease of conductivity is in that case the progressive trapping of the charge carriers by Fe(III). Consequently, the conductivity of the phase $x = 1.2$ has not significantly changed with respect to the pristine cuprate, i.e., remains close to 10^3 $(\Omega \cdot \text{cm})^{-1}$ at room temperature (Table 5), and is characteristic of a semimetal.

Finally, the fact that in the second series the conductivity at room temperature of the annealed compounds does not decrease dramatically with respect to the pristine phase suggests that the transport properties of this phase are anisotropic, with a semimetallic behavior along **c**, and a semiconducting behavior in the (**ab**) plane, in agreement with the ordered substitution of iron for copper deduced from the structural study.

CONCLUDING REMARKS

The ordered substitution of iron for copper in the $La_{8-y}Sr_yCu_8O_{20}$ structure has been demonstrated for the first time. The role of the hole carrier density, introduced by the presence of Cu(III), has been elucidated by comparing two series of oxides with and without compensation. These results suggest that such materials should exhibit anisotropic transport properties. A systematic neutron diffraction study will be performed to get a better understanding of the "Fe–Cu–O" framework.

REFERENCES

1. J. M. Tarascon, P. Barboux, P. F. Miceli, L. H. Greene, G. W. Hull, M. Eibschutz, and S. A. Sunshine, *Phys. Rev. B* **37,** 7458 (1988).
2. G. Xiao, F. H. Streitz, A. Garvin, Y. W. Du, and C. L. Chien, *Phys. Rev. B* **35,** 8782 (1987).
3. J. L. Garcia-Muñoz, J. Rodriguez Carvajal, S. H. Kilcoyne, C. J. Boardman, and R. Cywinki, *J. Magn. Magn. Mater.* **104–107,** 555 (1992).

4. I. Mirebeau, C. Bellouard, M. Hennion, V. Caignaert, and E. Suard, *J. Appl. Phys.* **73,** 5689 (1993).
5. I. Mirebeau, E. Suard, V. Caignaert, and F. Bourée, *Phys. Rev. B* **50,** 3230 (1994).
6. L. Er-Rakho, C. Michel, and B. Raveau, *J. Solid State Chem.* **73,** 514 (1988).
7. C. Michel, L. Er-Rakho, and B. Raveau, *J. Phys. Chem. Solids* **49**(4), 451 (1988).
8. D. B. Wiles and R. A. Young, *J. Appl. Crystallogr.* **540,** 259 (1981).
9. L. Er-Rakho, Thesis, Université de Caen, and France, 1987.
10. L. Er-Rakho, C. Michel, Ph. Lacorre, and B. Raveau, *J. Solid State Chem.* **73,** 531 (1988).